Research Article

Abozer Y. Elderdery*, Abdulaziz H. Alhamidi, Ahmed M. E. Elkhalifa, Maryam M. Althobiti, Entesar M. A. Tebien, Nawal Eltayeb Omer, Siddiqa M. A. Hamza, Fehaid Alanazi, Badr Alzahrani, Suresh Kumar Subbiah, and Pooi Ling Mok

Synthesis and characterization of ZnO–TiO_2–chitosan–escin metallic nanocomposites: Evaluation of their antimicrobial and anticancer activities

https://doi.org/10.1515/gps-2022-0086
received July 07, 2022; accepted October 01, 2022

Abstract: This work intended to formulate bio-nanocomposites of zinc oxide (ZnO), titanium oxide (TiO_2), chitosan, and escin, characterize their physical properties, and evaluate their antimicrobial and anticancer properties. X-ray diffractometers (XRD) and scanning and transmission electron microscopes were applied to characterize the morphology and ultrastructure of chemically synthesized bio-nanocomposites. To investigate the functional groups of bio-nanocomposites, we used Perkin–Elmer spectrometers for Fourier transform infrared (FTIR) analysis and photoluminescence (PL) spectroscopy for PL spectrum analysis. Antimicrobial activities against bacterial and fungal strains were tested with agar well diffusion. Bio-nanocomposites were tested for anticancer effects on a MOLT4 blood cancer cell line using morphological analysis, methyl thiazole tetrazolium assay, apoptosis by acridine orange/ethidium bromide, and mitochondrial membrane potential ($\Delta\Psi m$). In XRD, FTIR, and PL, the active compounds of ZnO–TiO_2, chitosan, and escin peaks were observed. Our bio-nanocomposites demonstrated antimicrobial activity against bacterial and fungal pathogens. The bio-nanocomposite was cytotoxic to MOLT4 cells at an IC_{50} concentration of 33.4 $\mu g \cdot mL^{-1}$. Bio-nanocomposites caused cytotoxicity, changes in cell morphology, and mitochondrial membrane potential degradation, all of which resulted in apoptotic cell death. MOLT4 cells were found to be responsive to bio-nanocomposites based on ZnO–TiO_2–chitosan–escin.

Keywords: zinc oxide, titanium oxide, chitosan, escin, bio-nanocomposite, blood cancer

*** Corresponding author: Abozer Y. Elderdery,** Department of Clinical Laboratory Sciences, College of Applied Medical Sciences, Jouf University, Sakaka, Saudi Arabia; Health Sciences Research Unit, Jouf University, Sakaka, Saudi Arabia, e-mail: ayelderdery@ju.edu.sa
Abdulaziz H. Alhamidi: Clinical Laboratory Sciences Department, College of Applied Medical Science, King Saud University, Riyadh, Saudi Arabia
Ahmed M. E. Elkhalifa: Department of Public Health, College of Health Sciences, Saudi Electronic University, Riyadh, Kingdom of Saudi Arabia; Department of Haematology, Faculty of Medical Laboratory Sciences, University of El Imam El Mahdi, Kosti, Sudan
Maryam M. Althobiti, Entesar M. A. Tebien: Department of Clinical Laboratory Science, College of Applied Medical Sciences, Shaqra University, Shaqra, Saudi Arabia
Nawal Eltayeb Omer: Hereditary Blood Disease Center, Al Ehsaa, Saudi Arabia
Siddiqa M. A. Hamza: Department of Pathology, College of Medicine, Umm Alqura University, Algunfuda, Saudi Arabia
Fehaid Alanazi: Department of Clinical Laboratory Sciences, College of Applied Medical Sciences Al Qurayyat, Jouf University, Sakaka, Saudi Arabia
Badr Alzahrani: Department of Clinical Laboratory Sciences, College of Applied Medical Sciences, Jouf University, Sakaka, Saudi Arabia
Suresh Kumar Subbiah: Centre for Materials Engineering and Regenerative Medicine, Bharath Institute of Higher Education and Research, Chennai, India
Pooi Ling Mok: Department of Biomedical Science, Faculty of Medicine and Health Sciences, Universiti Putra Malaysia, 43400 UPM Serdang, Selangor, Malaysia
ORCID: Abozer Y. Elderdery 0000-0002-6219-5312

1 Introduction

The high mortality rate is still recorded due to emerging and re-emerging diseases despite major leaps in the development of pharmaceutical drugs to treat a range of infectious or non-infectious diseases [1]. The development of effective and inexpensive drugs is aimed at limiting the economic and social burden of these diseases. Nanotechnology has gained attention in a variety of fields, including bioengineering, medical applications, clinical drug development, and imaging studies [2,3]. Notably, the nanotechnology

platform has positively contributed to the treatment of rare disease conditions such as hereditary transthyretin amyloidosis via siRNA-based delivery to silent the gene responsible for the disease [4]. Similarly, in recent days, numerous researchers have focused on developing nanoparticle or nanocomposite-based drugs and testing their efficacy in various human disease conditions including cancer [5], diabetes [6], and neurodegenerative conditions [7]. Indeed, the investigation of nanoforms of plant-derived phytochemicals has gained significant attention to develop drugs for cancer and various other human diseases affecting the communities [8].

Leukemia comprises malignancies of blood cells derived from blood-forming tissues in the bone marrow [9]. In the past three decades, the incidence of leukemia has risen rapidly, and the demand for drug resources to combat it is highly warranted [10]. Although many drugs have been developed and tested in leukemic patients, the treatment remains challenging and mortality is inevitable [11], mainly due to the development of resistance to drug treatments and metastasis of leukemic cells [12]. Notably, the progression of drug resistance in leukemic cells was found to originate from leukemia stem cells (LSCs). Several factors responsible for the failure to target drug-resistant leukemia cells with drug formulations have been reviewed in detail [13,14]. Currently, to test the efficacy of new drug candidates against leukemia, a human T lymphoblast cell line also known as high migrating drug-surviving MOLT4 cells has been used across various laboratories in leukemia research [15,16].

Escin is a phytochemical constituent of the traditional medicinal plant *Aesculus hippocastanum* (horse chestnut) [17]. It has been used to treat rectal hemorrhoids and hematomas and exhibits other pharmacological benefits like anti-inflammatory, anticancer, and cardioprotective properties in diabetic experimental models [18–20]. This study has characterized the physicochemical of a newly synthesized drug candidate using Zn, TiO_2, and chitosan conjugated with escin and identified its potential as an antimicrobial and *in vitro* anti-tumoral agent on the MOLT4 blood cancer. For the latter purpose, the ability of synthesized nanoparticles to induce apoptosis and increase reactive oxygen species (ROS) production in MOLT4 cells will be assessed.

2 Materials and methods

2.1 Chemicals and their sources

Escin, copper oxide, titanium oxide, and acridine orange/ethidium bromide (AO/EtBr) staining kit were purchased from Sigma chemical company. Cell culture media (RPMI-1640 Medium), antibiotic penicillin/streptomycin, and FBS were obtained from Hi-Media Laboratories, Mumbai, India. Antibiotic discs, amoxicillin, dimethylsulfoxide (DMSO), potato dextrose agar (PDA), nutrient agar for bacterial culture, paraformaldehyde (PFA), coverslips, Tween-20, poly-L-lysine, and sterile PBS (with and without Ca, Mg) was procured from Sigma, USA, Hi-Media Laboratories and Merck chemical company, Germany.

2.2 Bio-nanocomposite of ZnO, TiO_2, chitosan, and ecin synthesized chemically

Synthesis of ZnO–TiO_2-chitosan-escin was carried out using a chemical precipitation procedure as follows. A solution of 100 mM Zn $(NO_3)_2{\cdot}6H_2O$ was mixed with 50 mL of 1% acetic acid, and 500 mg of titanium dioxide nanoparticles and 500 mg of chitosan were mixed one by one. In addition, 50 mg phytocomponent escin was mixed with ZnO–TiO_2–chitosan solution. Then, 100 mM of NaOH solution was gently mixed with 50 µL of ZnO–TiO_2–chitosan–escin solution until a white residue was formed. The residue was heated at room temperature for 3 h along with constant stirring using a magnetic stirrer. We rinsed the nanopowder three to four times with distilled water and ethanol solutions. Following centrifugation at 15,000 rpm for 40 min at –3°C, the final reaction solvent was dehydrated at 200°C for 2 h before characterization analyses.

2.3 Physicochemical analysis of ZnO–TiO_2–chitosan–escin nanocomposites

ZnO–TiO_2–chitosan–escin bio-nanocomposites obtained from our synthesis procedure were subjected to physicochemical analysis using an X-ray diffractometers (XRD) (model: X'PERT PRO PANalytical). The diffraction patterns were documented in the 2θ range of between 25°C and 80°C for ZnO–TiO_2–chitosan–escin bio-nanocomposite, with a monochromatic CuKα diffraction beam of wavelength 1.5406 Å. An field emission scanning electron microscope (FE-SEM; Carl Zeiss Ultra 55 FESEM) with energy-dispersive X-ray spectroscopy (model: Inca) was used to analyze the ZnO–TiO_2–chitosan–escin bio-nanocomposite. The morphologies of the ZnO–TiO_2–chitosan–escin bio-nanocomposite were studied using a transmission

electron microscopy (TEM; Tecnai F20 model) with a 200 kV accelerating voltage. The Fourier transform infrared (FTIR) spectra were acquired with a Perkin–Elmer spectrometer in the wavenumber range 400–4,000 cm^{-1} [21]. The absorption spectra of the ZnO–TiO_2–chitosan–escin bio-nanocomposite were examined through a Lambda 35 spectrometer between 200 and 1,100 nm [22]. Perkin Elmer-LS 14 spectrometer was used to capture photoluminescence (PL) spectra.

2.4 Bacterial growth inhibitory studies

A well diffusion approach was utilized to investigate the antibacterial capacity of the formulated ZnO–TiO_2–chitosan–escin bio-nanocomposite. Bacterial strains from Gram-positive strains (*S. aureus* and *B. subtilis*) and Gram-negative strains (*P. aeruginosa* and *E. coli*) were employed. In this investigation, strains were inoculated individually on sterile Mueller Hinton agar containing Petri discs. The antibacterial activity of a ZnO–TiO_2–chitosan–escin bio-nanocomposites at 1, 1.5, and 2 $mg{\cdot}mL^{-1}$ dispersed in a 5% sterile dimethyl sulfoxide (DMSO) solution was demonstrated. The plates were maintained for 24 h at 37°C, and then inhibition zones were determined after 24 h. Amoxicillin antibiotic (30 $\mu g{\cdot}mL^{-1}$) was utilized as positive drug, and the tests were performed in triplicates.

2.5 Antifungal properties

The antifungal potential of *Candida albicans* was assessed using standard procedures as reported earlier and growth on PDA [23]. The *C. albicans* strain was injected onto the PDA agar petri plate by streaking twice or thrice, followed by moving the plates in a circular plane at an angle of 60° for each streak to ensure homogeneity in the inoculums spreading. Following that, germ-free forceps were used to put wells containing 1, 1.5, and 2 $\mu g{\cdot}mL^{-1}$ of test ZnO–TiO_2–chitosan–escin bio-nanocomposite onto the inoculation plates, which were then sustained at 30°C for 24 h under visible light. Following the incubation of *C. albicans* with synthesized bio-nanocomposites, the inhibition zones were determined to assess the growth inhibitory efficacy of ZnO–TiO_2–chitosan–escin bio-nanocomposite. The amoxicillin (30 $\mu g{\cdot}mL^{-1}$) was employed as a positive control. Experiments were performed in triplicates.

2.6 Cell culture and maintenance

MOLT4 cells were grown in a humidified room using RPMI-1640 medium enriched with 10% of FBS and 1% of penicillin-streptomycin antibiotic. Subcultured cells were loaded at the population of around 4×10^5 $cells{\cdot}mL^{-1}$. As soon as the cells reached confluence, they were immediately subcultured into fresh cell culture dishes according to the experiment's requirements. MOLT4 cells were fed fresh RPMI-1640 media every 2–3 days, depending on the cell density.

2.7 Methyl thiazole tetrazolium assay for cell viability

Cytotoxicity of the synthesized bio-nanocomposites on the MOLT4 cancer cells was carried out by using MTT assay. MOLT4 cells were first grown on 96-well clear-bottom plates at a population of 1×10^4 $cells{\cdot}well^{-1}$. After 24 h, the MOLT4 cells were administered with bio-nanocomposites at various doses (10, 20, 30, 40, 50, and 60 $\mu g{\cdot}mL^{-1}$) for 72 h. Following the treatment period, cells were cleansed with sterile PBS, and 20 µL of MTT was mixed in each well and further sustained for 4 h, with regular monitoring under an inverted microscope for the production of blue-colored formazan crystals. After the development of formazan stones, the media was removed from wells and added with 150 µL of DMSO to solubilize the formazan. The plates were rotated on an orbital shaker to obtain a uniform solution. The OD was quantified using a plate reader at 570 nm. MTT assay was performed following procedures reported previously and with required modifications for our study [24]. The results of OD were utilized to determine the IC_{50} values, and the percentage of cell death is quantified using the formula:

$$\text{Cell death}(\%) = (1 - \text{Sample } A_{570}/\text{Control } A_{570}) \times 100\% \quad (1)$$

2.8 Cell morphological analysis and staining with AO/EtBr

MOLT4 cells at a population of 1.5×10^5 $cells{\cdot}well^{-1}$ were seeded and cultured in 12-well plates overnight. MOLT4 cells were then supplemented with 30 and 40 $\mu g{\cdot}mL^{-1}$ of bio-nanocomposites for 24 h. After that, the cells were cleansed using PBS and proceeded for morphological analysis and staining with AO/EtBr dyes. For morphological

analysis, the cells were immobilized using 4% PFA in PBS for 10 min. The morphological alterations were detected using an inverted phase-contrast microscope (Olympus Corporation). The PBS-washed MOLT4 blood cancer cells were also incubated using 1 µM AO/EtBr at 37°C for 15 min under dark conditions. Finally, the stained MOLT4 cells were observed and documented using a fluorescent microscope for the visualization of cells stained with the AO/EtBr dyes. Experiments were performed in triplicates.

2.9 Measurement of MMP level (ΔΨm)

MOLT4 cells were cultured onto the 24-well plate at a population of 2×10^5 cells·well^{-1} and treated for 24 h with IC_{50} concentrations (30 and 40 µg·mL^{-1}) of the bio-nanocomposite. The state of MMP was evaluated using the rhodamine-123 (Rh-123). Rh-123 penetrates the mitochondrial matrix and requires mitochondrial transmembrane potential to induce PL. MOLT4 cells were treated with 10 mM Rh 123 for 30 min before being cleansed thrice with PBS. Finally, the intensity of fluorescence was detected using a spectrofluorometer at 488 and 510 nm, respectively, as excitation and emission wavelengths. The fraction of control cells with MMP was calculated.

2.10 Nuclear fluorescence labeling on MOLT4 cells to detect nuclear damage

The morphology of nucleic acid material was examined using fluorescence microscopy using the morphology of nucleic aci staining technique [25]. A population of 1×10^4 cells·well^{-1} was used for the seeding of MOLT4 cells in the bottom dish. An atmosphere of 5% CO_2 and 37°C humidified for 24 h was used for incubation. Incubated for another 24 h under the same conditions, the cells were then exposed to ZnO–TiO_2–chitosan–escin bio-nanocomposite concentrations (30 g and 40 µg·mL^{-1}) except for the control group. A DAPI solution (diluted in methanol) was added after the cells had been washed twice with 1× PBS. The plates were enclosed in aluminum foil to prevent light exposure and incubated for a further 15 min. Fluorescence microscopy was used to examine the nuclear material morphology (Biorad, ZOE fluorescent imaging system, Germany).

2.11 An assessment of ROS accumulation

To estimate the ROS accumulation using fluorescence microscopy, the dichloro-dihydro-fluorescin diacetate (DCFH-DA) staining technique was used. The MOLT4 cells were treated for 24 h with 30 and 40 µg of ZnO–TiO_2–chitosan–escin bio-nanocomposite, and the untreated cells served as controls. Roughly 2×10^5 of cells in 1 mL suspension was mixed with 10 µM DCFH-DA solution and allowed to incubate for 5 min at 37°C. After washing and resuspending the cells in PBS solution, the fluorescence images were acquired using a fluorescent microscope at 485 and 530 nm, respectively, as excitation and emission wavelengths.

2.12 Statistical analysis

Data were illustrated as mean ± SD, and the variance between the groups was calculated using a one-way ANOVA and DMRT tests. Statistically significant was determined as the p-value was less than 0.05.

3 Results

3.1 Characterization of ZnO–TiO_2–chitosan–escin bio-nanocomposites

ZnO–TiO_2–chitosan–escin bio-nanocomposites show X-ray diffraction characteristics in Figure 1. According to the XRD molecular patterns, ZnO was the major face found at angles (2θ) 31.76°, 34.41°, 36.24°, 47.55°, 56.54°, 62.78°, 66.36°, 68.11°, and 69.24° and corresponding hkl values were (100), (002), (101), (102), (110), (103), (200), (112), and (201) for ZnO (wurtzite hexagonal) phase formation, which matched with JCPDS card No. 36-1451. The angle 2θ peak of TiO_2 was noted at 25.06° and 29.58°, 43.97° it is marked by (#) revealing the anatase phase of the material (JCPDS card no. 21-1272). Chitosan diffraction peak was 10.52° and escin was 15.83°, which are characteristic of noncrystalline materials. According to the study, ZnO–TiO_2–chitosan–escin phases form as a result of hydrogen bonding between ZnO–TiO_2–chitosan–escin components and steric interactions during phase formation. As determined by Debye–Scherrer (Figure 1), the average crystallite size of bio-nanocomposites is 55 nm.

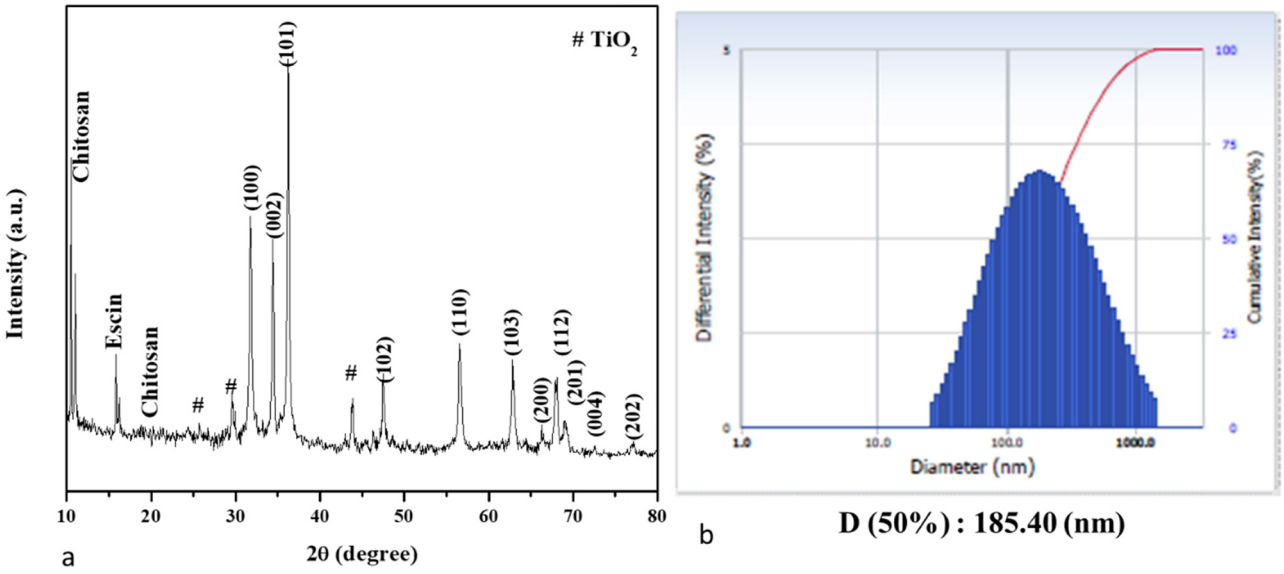

Figure 1: An XRD analysis (a) and DLS spectrum (b) of ZnO–TiO_2–chitosan–escin bio-nanocomposites are shown. Three replicates were performed and representative images are shown.

A FESEM analysis and TEM analysis of a ZnO–TiO_2–chitosan–escin bio-nanocomposite (Figure 2) and TEM analysis (Figure 3) were carried out to determine its surface morphology. ZnO, TiO_2, chitosan, and escin bio-nanocomposites were visualized using FESEM and TEM images, showing a nanorod structure with an average particle

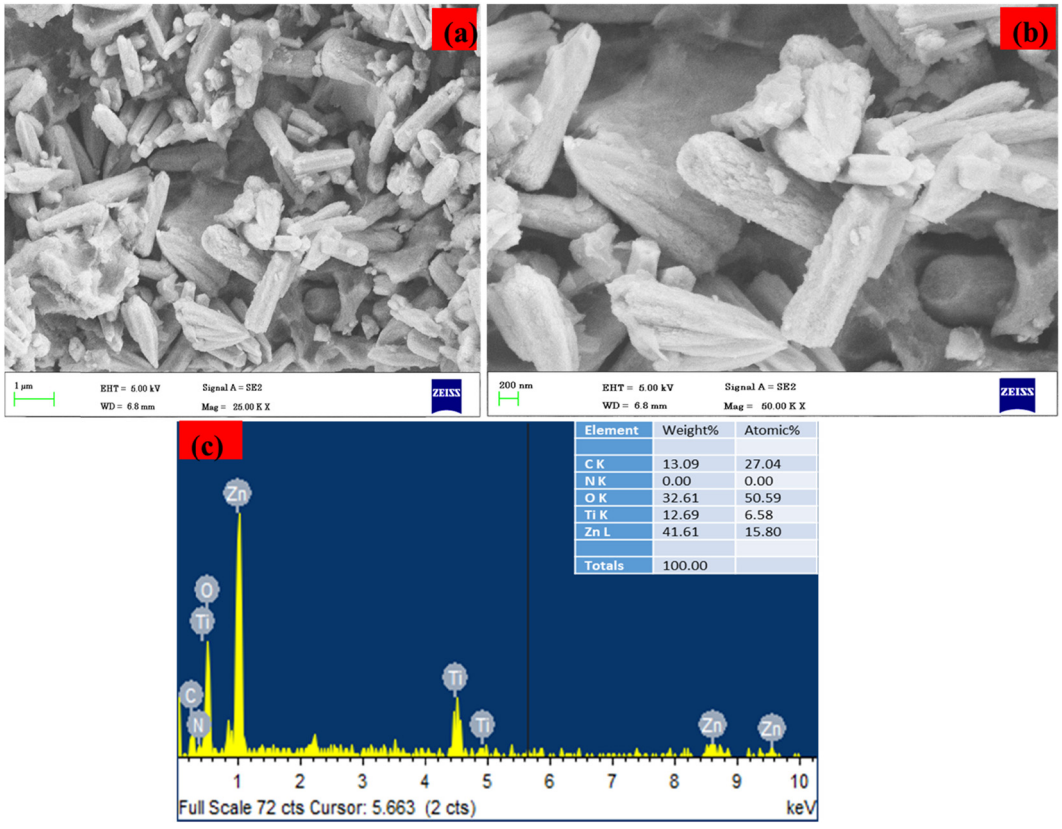

Figure 2: FESEM images of ZnO–TiO_2–chitosan–escin bio-nanocomposites: (a) lower and (b) higher magnifications, and (c) EDAX spectrum.

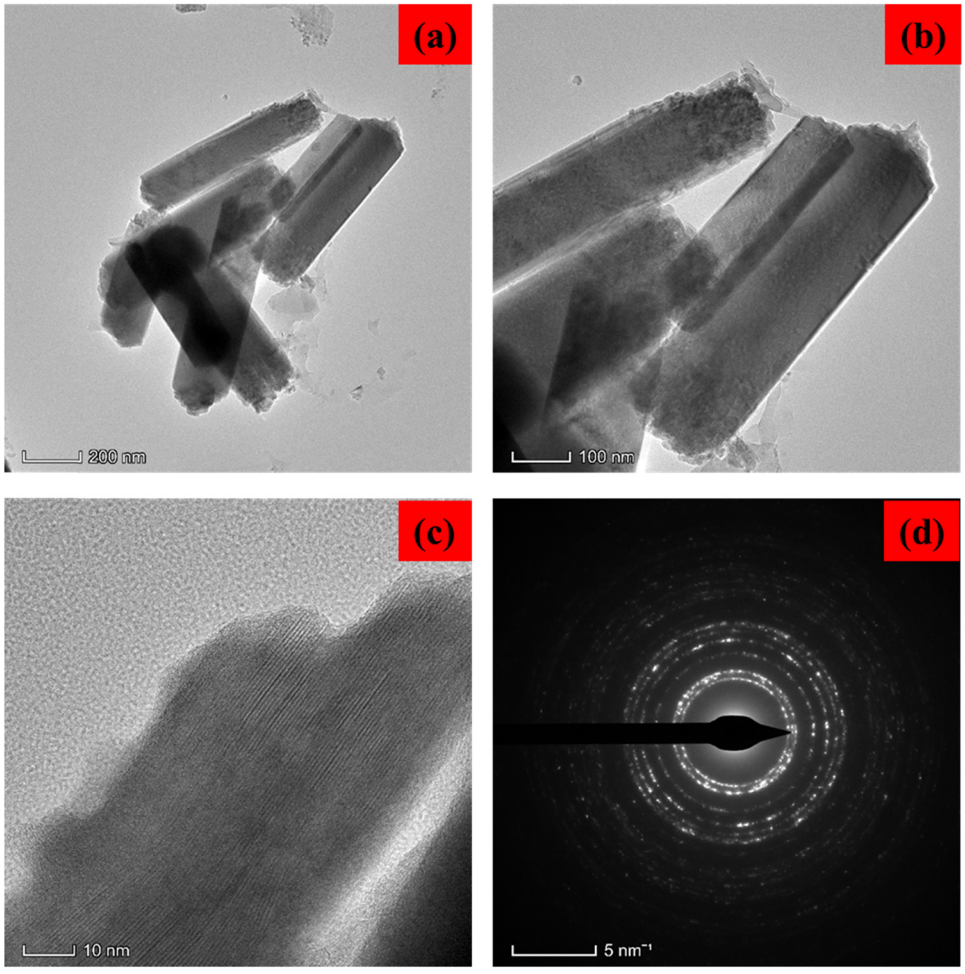

Figure 3: The TEM images of the ZnO–TiO_2–chitosan–escin bio-nanocomposites are shown in (a) lower and (b and c) higher magnifications. (d) selected area (electron) diffraction (SAED) patterns are shown by the bio-nanocomposites. A photomicrograph of a representative image is shown here.

size of 72 nm. The bio-nanocomposites were prepared from the SAED pattern (Figure 4d). EDAX spectrum of ZnO–TiO_2–chitosan–escin (Figure 2c) with 21.59% concentration of C, 5.45% of N, 15.80% of Zn, 6.58% of Ti, and 50.58% of O in the bio-nanocomposites ZnO–TiO_2–chitosan–escin was estimated.

In the ZnO–TiO_2–chitosan–escin samples, the FTIR spectrum revealed the presence of ZnO, TiO_2, chitosan, and escin functional groups. The broad –OH and –NH peaks with hydrogen bonds were detected in the chitosan peaks at 3,419 and 1,608 cm^{-1}, showing the amide I group (C–O stretching combined with the N–H deformation mode) (Figure 4). During the carbonic acid salt's stretching vibration, the COO^- group produced the peak at 1,384 cm^{-1}, and during the glucose circle's stretching vibration, the peak at 1,066 cm^{-1} was caused by the stretching vibration of C–O–C [26]. Escin's distinctive summits, on the other hand, are as follows: There were asymmetric and symmetric peaks in C–H group at 2,924 and 2,846 cm^{-1}, as well as C–O stretching and C–H out-of-plane bending peaks at 1,161 and 934 cm^{-1} [27]. The metal-oxygen (M–O) stretching vibration, similar to Zn–Ti–O, was discovered at 718 and 532 cm^{-1} [28]. The results of the FTIR spectrum suggest that the bio-nanocomposite performed effectively with the chitosan and escin molecules in the ZnO and TiO_2 surface matrices. These interactions were caused by the electrostatic interaction between the ZnO–TiO_2–chitosan–escin bio-nanocomposite (Figure 4).

Ultraviolet–Visible absorbance spectrum of the ZnO–TiO_2–chitosan–escin bio-nanocomposite dispersed in water is shown in Figure 4. The UV absorbance edge peak was centered at 370 nm for hexagonal wurtzite ZnO–TiO_2–chitosan–escin bio-nanocomposite [29]. The redshift (5 nm) was observed at the synthesized ZnO–TiO_2–chitosan–escin bio-nanocomposite absorbance peak as compared to that of bulk ZnO (365 nm) [30]. Because of foreign (TiO_2-chitosan-escin) molecules on

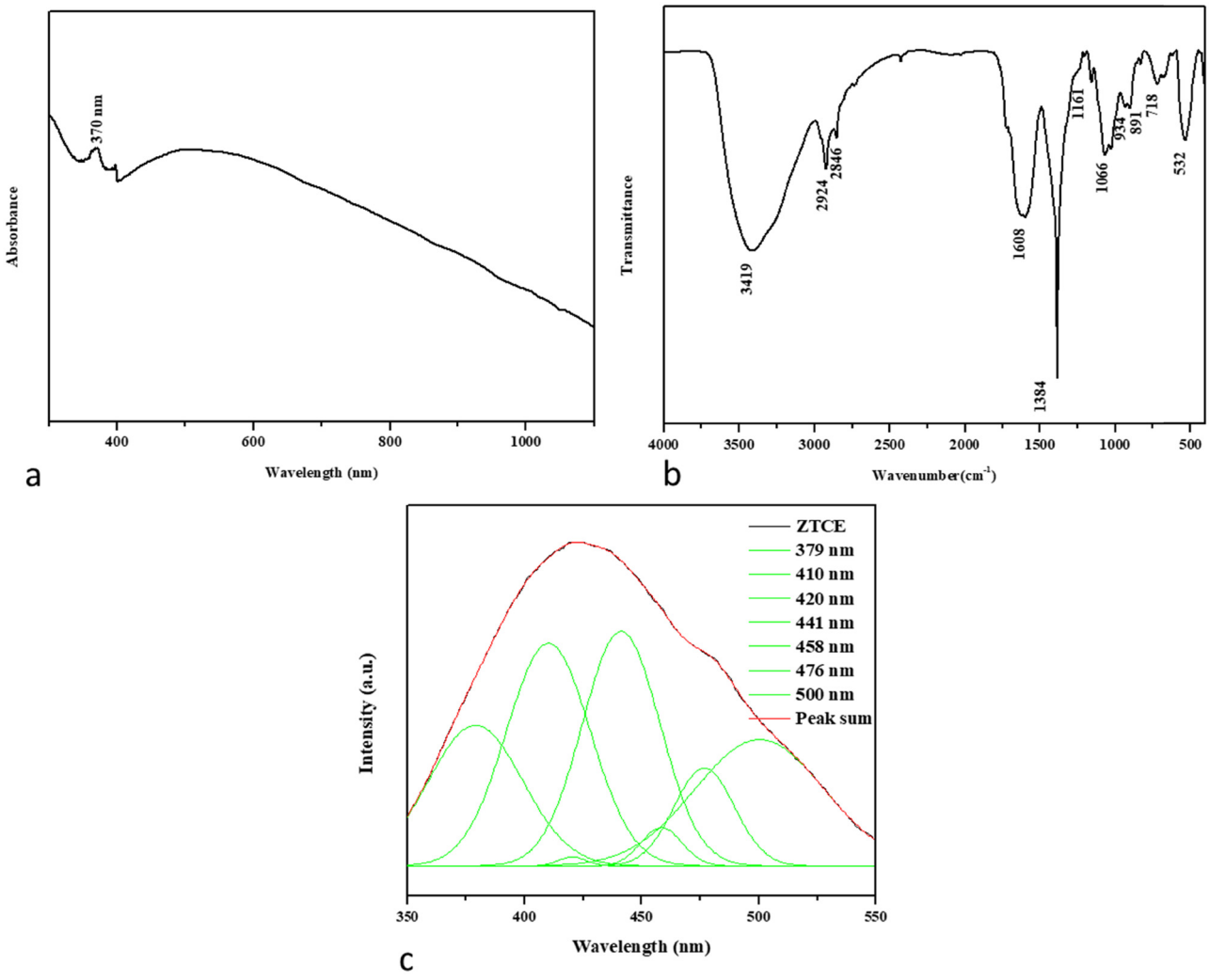

Figure 4: An analysis of ZnO–TiO_2–chitosan–escin bio-nanocomposites by (a) UV absorbance, (b) FTIR spectra, and (c) PL spectra. These data represented the results of experiments performed in triplicate.

the lattice surface, this redshift can be attributed to the development of shallow levels inside the bandgap [31]. The PL spectra of a synthesized ZnO–TiO_2–chitosan–escin bio-nanocomposite with an excitation wavelength of 325 nm are revealed in Figure 4. The ZnO–TiO_2–chitosan–escin bio-nanocomposite PL emission spectrum was found at 379, 410, 420, 441, 458, 476, and 500 nm, respectively (Figure 4). Near band edge emission at 379 nm was found, corresponding to the radiative recombination of the free exciton-exciton collision mechanism [32]. The violet emission seen at 410 nm could be caused by electron transfer from a surface donor level of zinc interstitials (Zn_i) to the top level of the valence band [26]. The three blue emission bands at 420, 441, 458, and 476 nm [26] represent singly ionized Zn vacancies (VZn). The green emission band at 500 nm could be caused by oxygen vacancies (O_v) [26].

3.2 ZnO–TiO_2–chitosan–escin bio-nanocomposite-induced antimicrobial activity

The antibacterial efficacy of the produced ZnO–TiO_2–chitosan–escin bio-nanocomposite was investigated using an agar well diffusion approach against (*S. aureus* and *B. subtilis*) as a gram-positive and (*P. aeruginosa* and *E. coli*) as a gram-negative bacterial strains and fungal *Candida albicans* infections (Figure 5). ZnO–TiO_2–chitosan–escin caused a zone of inhibition against gram-positive, gram-negative, and fungal strains, as shown in Figure 5. According to the findings, raising the concentration of ZnO–TiO_2–chitosan–escin bio-nanocomposite increased the widths of the inhibitory zones for all of the tested pathogens.

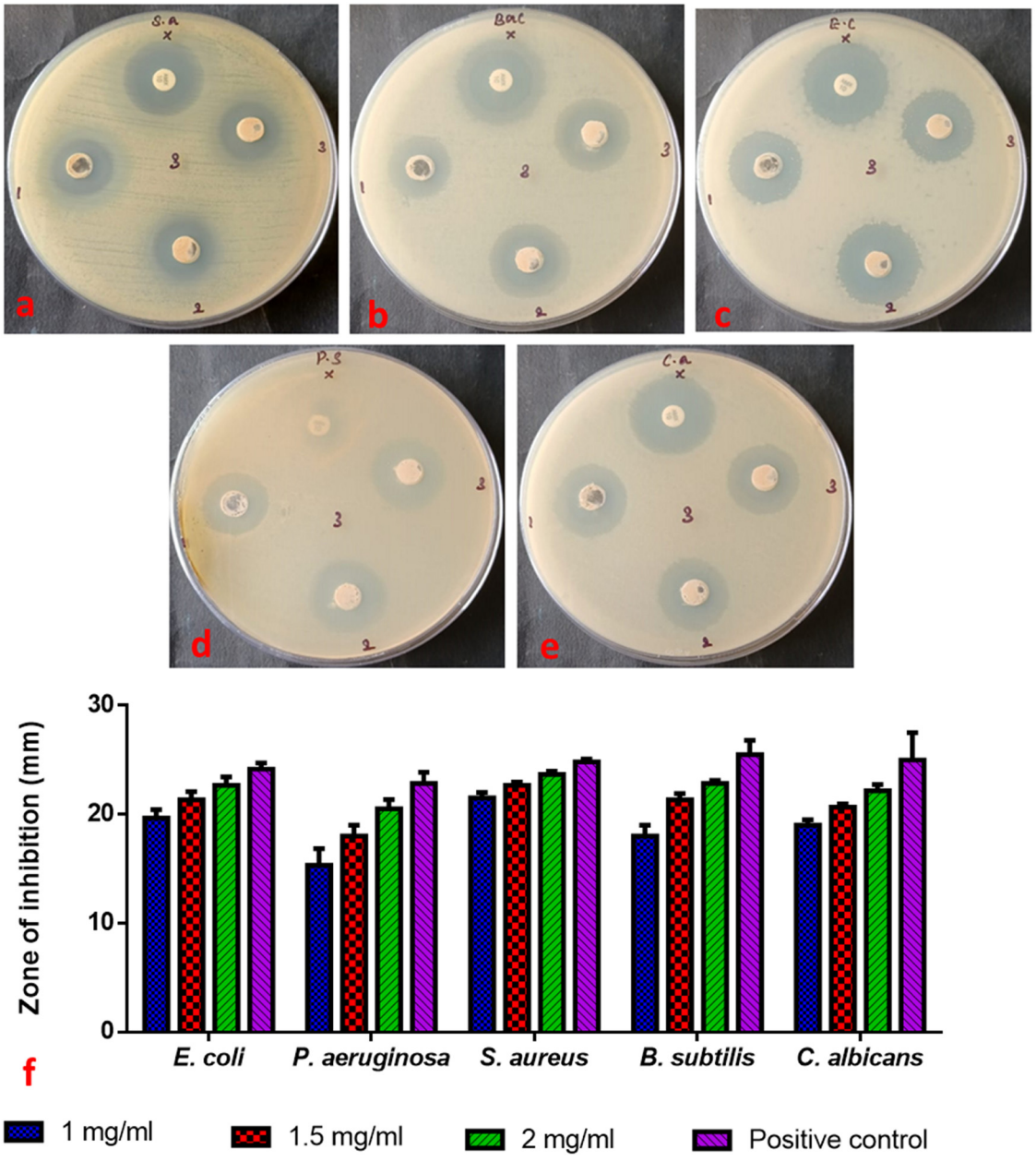

Figure 5: Antimicrobial activity of a ZnO–TiO_2–chitosan–escin bio-nanocomposites. These data were generated following the treatment of (a) *S. aureus*, (b) *B. subtilis*, (c) *E. coli*, (d) *P. aeruginosa*, and (e) *C. albicans* with the bio-nanocomposites. (f) The graph shows values of zones of inhibition. A representative set of data from the triplicate experiments is presented here.

3.3 ZnO–TiO_2–chitosan–escin bio-nanocomposite-induced cytotoxicity on MOLT4 cells

We performed an MTT assay to investigate the impacts of bio-nanocomposites on the MOLT4 cell line. In this study, the bio-nanocomposites exhibited cytotoxicity on MOLT4 cells at a 33.4 $\mu g \cdot mL^{-1}$ (IC_{50}) dose. Therefore, for all subsequent experiments testing its anticancer effect, we treated cells for 24 h with 30 and 40 $\mu g \cdot mL^{-1}$, following which we collected the drug-surviving cells (Figure 6).

3.4 Bio-nanocomposite-induced morphological changes in MOLT4 cells

Bio-nanocomposites were added to MOLT4 cells at a dose of 30 and 40 $\mu g \cdot mL^{-1}$ and incubated for 24 h. Following

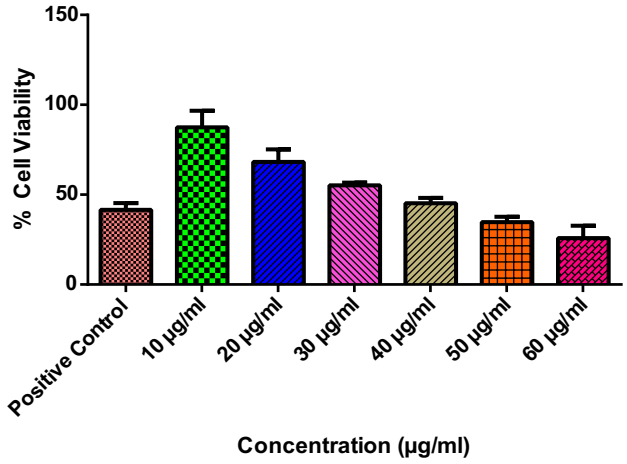

Figure 6: The experiment shows the results of a cell cytotoxicity assay using MTT and ZnO–TiO_2–chitosan–escin bio-nanocomposites at different concentrations (10, 20, 30, 40, 50, and 60 µg·mL^{-1}) in MOLT4 cells in 96-well plates. Experiments were performed in triplicate to determine the IC_{50} value, and representative data are shown here for the dose resulting in 50% inhibition of cell growth.

treatment, cells were visualized under a light microscope. Treatment with the bio-nanocomposites significantly reduced ($p < 0.05$) the population of the MOLT4 cells with changes in the morphology of the cells as compared to control untreated cells (Figure 7).

3.5 ZnO–TiO_2–chitosan–escin bio-nanocomposites-induced apoptosis in MOLT4 cells

Following a 24-h treatment with the bio-nanocomposites at a dose of 30 and 40 µg·mL^{-1}, MOLT4 cells were fixated, stained with AO/EtBr, and monitored using a fluorescence microscope. A green fluorescence signal indicating alive cells and free of apoptosis was detected by AO in the control cells; however, yellowish orange fluorescence was detected in the nanocomposite-treated cells, indicating earlier stage and late stage of apoptotic cell death, and condensation of nucleic acid and red fluorescence indicate the cell death was carried out by necrosis, respectively (Figure 8). The fluorescence intensity increased as the dosage of the nanocomposite increased (Figure 8). As a result, the capacity of nanocomposite to cause apoptosis in blood cancer cells became apparent.

3.6 ZnO–TiO_2–chitosan–escin bio-nanocomposites-induced nuclear changes in MOLT4 cells

By interacting with the cells, ZnO–TiO_2–chitosan–escin bio-nanocomposites altered cell permeability, aggregated, disrupted enzyme systems, and produced ROS. DAPI staining revealed intact nuclear morphology in the control panel, but condensed or fragmented morphology in treatment-treated cells (Figure 9). Morphological indicators of apoptosis, such as fragmented and condensed DNA, indicated the onset of cell death. The inhibition of cell cycle progression, the disruption of cell permeability, the accumulation of ROS, and stimulation of the caspase cascade all slowed down cell growth.

3.7 ZnO–TiO_2–chitosan–escin bio-nanocomposites-induced alteration in mitochondrial membrane potential (MMP, ΔΨm) on MOLT4 cells

In this investigation, it was observed that MMP was altered, as the control cells exhibited a brilliant green fluorescence, indicating a higher MMP level. However,

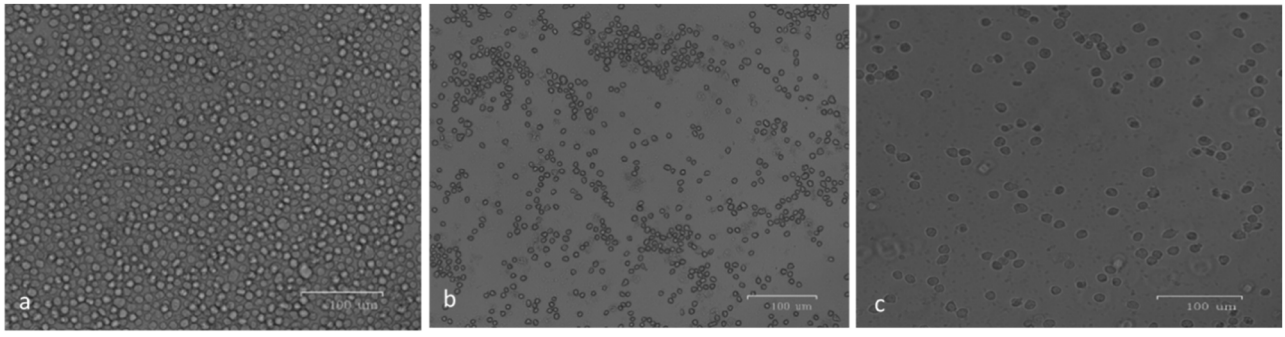

Figure 7: Morphological changes in MOLT4 cells after treatment for 24 h with ZnO–TiO_2–chitosan–escin bio-nanocomposite. (a) Untreated control cells, (b) cells treated with 30 µg·mL^{-1}, and (c) 40 µg·mL^{-1} of ZnO–TiO_2–chitosan–escin bio-nanocomposite. These are representative images of the experiment performed in triplicates with magnification at 20×.

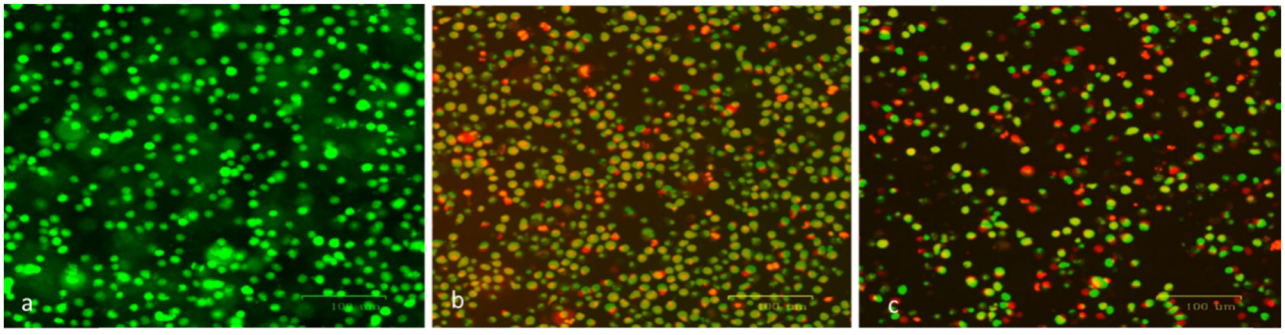

Figure 8: Apoptosis was determined in MOLT4 cells by using AO/EtBr dual staining following treatment with IC_{50} doses of ZnO–TiO_2–chitosan–escin bio-nanocomposites. Cells in green color indicated live cells, yellowish red color cells indicated early apoptotic cells, and red color cells indicated late apoptotic cells. (a) Untreated control cells, (b) cells treated with 30 μg·mL^{-1}, and (c) 40 μg·mL^{-1} of ZnO–TiO_2–chitosan–escin bio-nanocomposite. These are representative images of the experiment performed in triplicates with magnification at 20×.

MOLT4 cells treated with the nanocomposites showed dull or decreased green fluorescence, indicating that the cells' MMP was inhibited. This discovery indicated that nanocomposite could reduce MMP levels in MOLT4 cells, explaining the higher ROS levels (Figure 10).

3.8 ZnO–TiO_2–chitosan–escin bio-nanocomposites-induced production of ROS in MOLT4 cells

We used DCFH-DA staining to assess ROS expression in untreated cells and compared the results with the bio-nanocomposites-treated MOLT4 cells. The intensity of the bright fluorescent green color can be considered proportional to the level of ROS produced by the cells (Figure 11). In the experimental cell group treated with bio-nanocomposites at 40 μg·mL^{-1}, there was a greater expression of ROS. In the group of cells treated with bio-nanocomposites at 30 μg·mL^{-1}, ROS expression was remarkably reduced, whereas ROS was almost negligible in control cells.

4 Discussion

The requirement for effective drug candidates for various diseases of humans and plant species is in growing demand [33]. In recent days, due to the development of drug resistance, many effective drugs for infectious diseases [34] and cancer have become ineffective and turned out to be an economic loss for the pharmaceutical industries and worrisome for research communities [35]. In our study, we have synthesized the bio-nanocomposite drug-using bimetallic complex zinc (Zn) and titanium (TiO_2) complexed with chitosan and conjugated with a plant phytochemical escin, a component of traditional plant

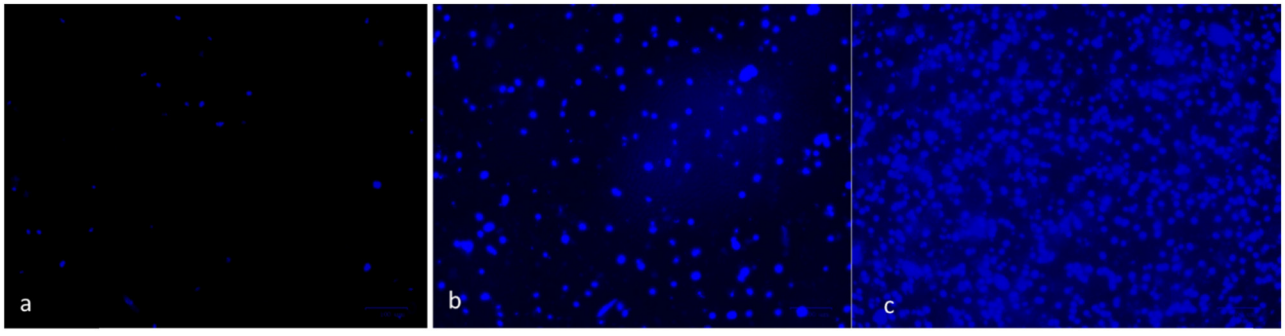

Figure 9: DAPI nuclear staining was used to determine apoptosis in MOLT4 cells after 24 h of treatment with IC_{50} doses of ZnO–TiO_2–chitosan–escin bio-nanocomposites. (a) Untreated control cells, (b) cells treated with 30 μg·mL^{-1}, and (c) 40 μg·mL^{-1} of ZnO–TiO_2–chitosan–escin bio-nanocomposite). These are representative images of the experiment performed in triplicates with magnification at 20×.

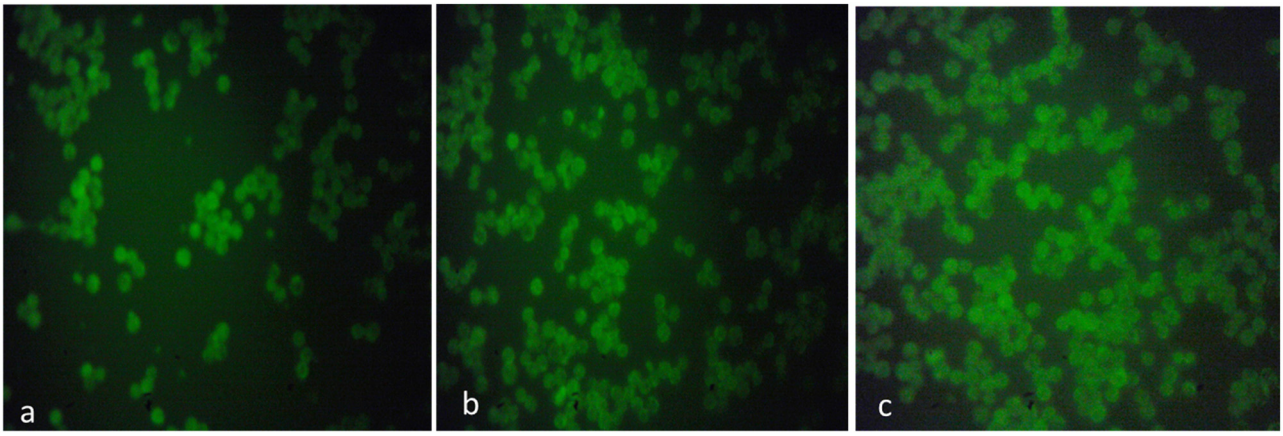

Figure 10: Dysfunction of mitochondrial membrane potential in MOLT4 cells after treatment with ZnO–TiO_2–chitosan–escin bio-nanocomposites. The mitochondrial membrane potential was determined by Rhodamine 123 nuclear staining. (a) Untreated control cells, (b) cells treated with 30 μg·mL^{-1}, and (c) 40 μg·mL^{-1} of ZnO–TiO_2–chitosan–escin bio-nanocomposites. These are representative images of the experiment performed in triplicates with magnification at 20×.

medicine *Aesculus hippocastanum*. Following the production of bio-nanocomposites, we have characterized the synthesized bio-nanocomposites to confirm their physical characteristics. Analysis using XRD, DLS, FESEM, TEM, EDAX spectrum, FTIR, and UV absorbance analysis all showed typical characteristics of a bio-nanocomposite as reported earlier with similar metallic complex and a plant phytoconstituents [36].

We additionally tested the bio-nanocomposites for antimicrobial potential against *P. aeruginosa*, *E. coli*, *S. aureus*, and *B. subtilis* bacteria and *Candida albicans* pathogen, using the agar well diffusion method. Our results showed escin bio-nanocomposites showed significant antibacterial and antifungal activity. The zone of inhibitions in antibacterial and antifungal analyses was significantly comparable to standard antibiotic treatments using amoxicillin. In our study, the observed antibacterial activity of bio-nanocomposites could be accredited to various causes, comprising: (1) the accumulation of bio-nanocomposites onto the bacterial cell surface, which caused the cell layer to be damaged and intracellular ingredients to be discharged; (2) development of Zn/Ti ions and their electrostatic interaction with the bacterial cell membrane; (3) formation and accumulation of reactive oxygen species, with oxidative potential that caused damage DNA and proteins of microbes. Titanium oxide can cause loss of membrane integrity by oxidizing phospholipids using hydroxyl radicals and causing membrane fluidity and loss of cellular contents, and eventually microbial cell lysis [37,38]. All these factors could cumulatively initiate the cell death phenomenon in bacterial and fungal cultures in our experimental analyses. A recent report that revealed the antibacterial activity of bio-nanocomposites made utilizing garlic extract, which is employed in commercial applications such as food preservation, supports our findings [39].

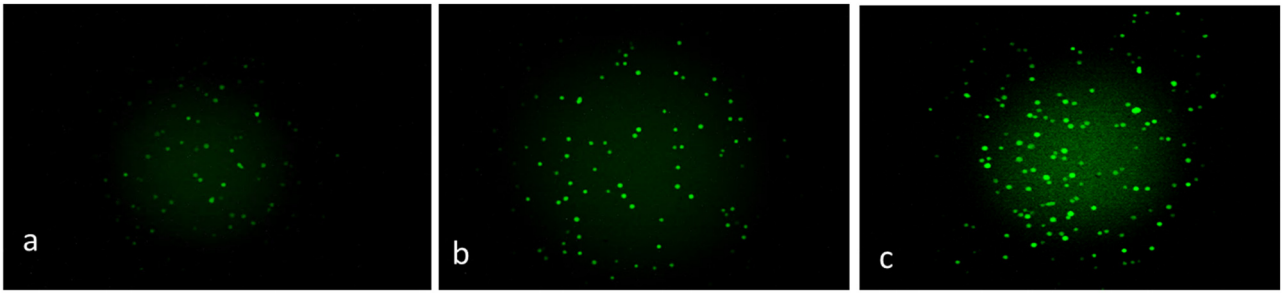

Figure 11: Fluorescence microscopic images of intracellular ROS generation induced by ZnO–TiO_2–chitosan–escin bio-nanocomposites in MOLT4 cells stained with DCFH-DA. (a) Untreated control cells, (b) cells treated with 30 μg·mL^{-1}, and (c) 40 μg·mL^{-1} of ZnO–TiO_2–chitosan–escin bio-nanocomposites. These are representative images of the experiment performed in triplicates with magnification at 20×.

Furthermore, we have tested the anticancer efficacy of nanocomposites using a MOLT4 blood cancer cell line, an *in vitro* experimental model. Treatment for leukemia is highly challenging due to the development of LSCs. LSCs have been found to participate in the progression of drug resistance in leukemic patients, rendering the patients and drug researchers in challenging conditions for reducing mortality rate [40]. MOLT4 cells treated using escin bio-nanocomposites showed significant cytotoxicity and loss of morphological architecture along with a substantial diminution in the total number of MOLT4 cells in culture plates. This denotes the escin bio-nanocomposites were capable of inducing cytotoxicity probably via the generation of ROS and pro-oxidants to trigger oxidative stress following penetration into the cells. Our observations demonstrated that the addition of Escin bio-nanocomposites in MOLT4 cells for 24 h induced a higher number of apoptotic cells, as shown in AO/EtBr staining, and increased the expression of ROS and loss of MMP. The study indicating that TiO_2 colloidal nanocomposite alone is capable of triggering cell death in leukemia cell line U937 *in vitro* is in agreement with our findings [41]. It is also possible that ZnO–TiO_2–chitosan–escin bio-nanocomposites escalated oxidative stress while contrarily blocking NF-kB cascade. Many anticancer drugs confer drug resistance to cancer cells by activating NF-kB and activating anti-apoptotic pathways [42]. Interestingly, nanocomplexes using selenium have been shown to inhibit nF-kB p65 in hepatic inflammatory conditions [43]. In the near future, this could be the possible aspect to examine the antitumor effect of escin bio-nanocomposites generated in our study.

5 Conclusion

This study used a green synthesis method to create a ZnO–TiO_2–chitosan–escin bio-nanocomposites. Following that, we investigated their anticancer potential by inhibiting cell growth and promoting apoptosis in MOLT4 cells. The bio-nanocomposites modified mitochondrial membrane potential and increased ROS generation *in vitro*. In addition, treatment with bio-nanocomposites increased the activation of apoptotic cell death. Further, it also showed antimicrobial effects on the growth of different pathogenic species in our *in vitro* experimental models. Hence, we recommended escin ZnO–TiO_2–chitosan complex bio-nanocomposites for further evaluation in drug testing studies and designing new drugs using various plant phytochemicals. The findings confirmed that bio-nanocomposites of ZnO–TiO_2–chitosan–escin could be potentially used to treat various leukemia and boost immune system functions.

Funding information: This research was funded by the Deanship of Scientific Research at Jouf University for financial support (DSR-2021-01-0355).

Author contributions: Abozer Y. Elderdery, Abdulaziz H. Alhamidi: writing – original draft, funding; Ahmed M. E. Elkhalifa, Maryam M. Althobiti, Entesar M. A. Tebien: writing – review and editing, methodology, formal analysis; Nawal Eltayeb Omer, Siddiqa M. A. Hamza, Fehaid Alanazi, Badr Alzahrani: study design, data analysis, formal analysis, visualization; Suresh Kumar Subbiah, Pooi Ling Mok: project administration.

Conflict of interest: The authors declare no conflict of interest.

Data availability statement: The corresponding author will provide the data upon reasonable request.

References

[1] Bui VKH, Park D, Lee YC. Chitosan combined with ZnO, TiO_2 and Ag nanoparticles for antimicrobial wound healing applications: A mini review of the research trends. Polym (Basel). 2017 Jan 9;9(1):21. PMID: 30970696; PMCID: PMC6432267. doi: 10.3390/polym9010021.

[2] Koo OM, Rubinstein I, Onyuksel H. Role of nanotechnology in targeted drug delivery and imaging: A concise review. Nanomedicine. 2005 Sep;1(3):193–212. PMID: 17292079. doi: 10.1016/j.nano.2005.06.004.

[3] Gaharwar AK, Peppas NA, Khademhosseini A. Nanocomposite hydrogels for biomedical applications. BiotechnolBioeng. 2014;111(3):441–53. doi: 10.1002/bit.25160.

[4] Adams D, Gonzalez-Duarte A, O'Riordan WD, Yang CC, Ueda M, Kristen AV, et al. Patisiran, an RNAi Therapeutic, for Hereditary Transthyretin Amyloidosis. N Engl J Med. 2018 Jul 5;379(1):11–21. PMID: 29972753. doi: 10.1056/NEJMoa1716153.

[5] Yuan X, He Y, Zhou G, Li X, Feng A, Zheng W. Target challenging-cancer drug delivery to gastric cancer tissues with a fucose graft epigallocatechin-3-gallate-gold particles nanocomposite approach. J Photochem Photobiol B. 2018 Jun;183:147–53. Epub 2018 Apr 17 PMID: 29705507. doi: 10.1016/j.jphotobiol.2018.04.026.

[6] Rongrong H, Tao Y, Ying K, Fang J, Wei J, Qiang Y, et al. Tin oxide-chitosan-polyethylene glycol-d-pinitol nanocomposite ameliorates cardiac ischemia in diabetic rats via activating p62/Keap1/Nrf2 signaling. J King Saud Univ - Sci. 2022 Apr 1;34(3):101827.

[7] Zhao Y, Cai J, Liu Z, Li Y, Zheng C, Zheng Y, et al. Nanocomposites inhibit the formation, mitigate the neurotoxicity, and facilitate the removal of β-amyloid aggregates in Alzheimer's disease mice. Nano Lett. 2019 Feb 13;19(2):674–83. Epub 2018 Nov 20 PMID: 30444372. doi: 10.1021/acs.nanolett.8b03644.

[8] Kaplan A. The nanocomposites designs of phytomolecules from medicinal and aromatic plants: promising anticancer-antiviral applications. Beni Suef Univ J Basic Appl Sci. 2022;11(1):17. doi: 10.1186/s43088-022-00198-z.

[9] Kantarjian HM, Keating MJ, Freireich EJ. Toward the potential cure of leukemias in the next decade. Cancer. 2018 Nov 15;124(22):4301–13. doi: 10.1002/cncr.31669.

[10] Yi M, Li A, Zhou L, Chu Q, Song Y, Wu K. The global burden and attributable risk factor analysis of acute myeloid leukemia in 195 countries and territories from 1990 to 2017: estimates based on the global burden of disease study 2017. J Hematol Oncol. 2020 Jun 8;13(1):72. PMID: 32513227; PMCID: PMC7282046. doi: 10.1186/s13045-020-00908-z.

[11] Li B, Tang H, Cheng Z, Zhang Y, Xiang H. The current situation and future trend of leukemia mortality by sex and area in China. Front Public Health. 2020 Dec 11;8:598215. PMID: 33363091; PMCID: PMC7759534. doi: 10.3389/fpubh.2020.598215.

[12] Huang X, Xiong M, Jin Y, Deng C, Xu H, An C, et al. Evidence that high-migration drug-surviving MOLT4 leukemia cells exhibit cancer stem cell-like properties. Int J Oncol. 2016;49:343–51.

[13] Zhang J, Gu Y, Chen B. Mechanisms of drug resistance in acute myeloid leukemia. Onco Targets Ther. 2019;12:1937–45. doi: 10.2147/OTT.S191621.

[14] Zawitkowska J, Lejman M, Drabko K, Zaucha-Prażmo A, Płonowski M, Bulsa J, et al. First-line treatment failure in childhood acute lymphoblastic leukemia: The polish pediatric leukemia and lymphoma study group experience. Med (Baltim). 2020 Feb;99(7):e19241. PMID: 32049864; PMCID: PMC7035074. doi: 10.1097/MD.0000000000019241.

[15] Karimi S, Mahdavi Shahri M. Medical and cytotoxicity effects of green synthesized silver nanoparticles using Achillea millefolium extract on MOLT-4 lymphoblastic leukemia cell line. J Med Virol. 2021 Jun;93(6):3899–906. doi: 10.1002/jmv.26694.

[16] Koszałka P, Stasiłojć G, Miękus-Purwin N, Niedźwiecki M, Purwin M, Grabowski S, et al. The Cooperative Anti-Neoplastic Activity of Polyphenolic Phytochemicals on Human T-Cell Acute Lymphoblastic Leukemia Cell Line MOLT-4 *In Vitro*. Int J Mol Sci. 2022 Apr 26;23(9):4753. doi: 10.3390/ijms23094753.

[17] Gallelli L. Escin: A review of its anti-edematous, anti-inflammatory, and venotonic properties. Drug Design Dev Ther. 2019;13:3425–37. doi: 10.2147/DDDT.S207720.

[18] Patlolla JMR, Rao CV. Anti-inflammatory and Anti-cancer Properties of β-Escin, a Triterpene Saponin. Curr Pharmacol Rep. 2015;1:170–8. doi: 10.1007/s40495-015-0019-9.

[19] Suryavanshi SV, Kulkarni YA. Attenuation of cardiac autonomic neuropathy by escin in diabetic rats. Pharmacology. 2021;106(3–4):211–7. Epub 2020 Sep 2 PMID: 32877906. doi: 10.1159/000509730.

[20] Amina M, Al Musayeib NM, Al-Hamoud GA, Al-Dbass A, El-Ansary A, Ali MA. Prospective of biosynthesized L. satiVum oil/PEG/Ag-MgO bionanocomposite film for its antibacterial and anticancer potential. Saudi J Biol Sci. 2021 Oct;28(10):5971–85. doi: 10.1016/j.sjbs.2021.06.052.

[21] Jihad MA, Noori F, Jabir MS, Albukhaty S, AlMalki FA, Alyamani AA. Polyethylene glycol functionalized graphene oxide nanoparticles loaded with nigella sativa extract: A smart antibacterial therapeutic drug delivery system. Molecules. 2021;26(11):3067.

[22] Bahjat HH, Ismail RA, Sulaiman GM, Jabir MS. Magnetic field-assisted laser ablation of titanium dioxide nanoparticles in water for anti-bacterial applications. J Inorg Organomet Polym Mater. 2021;31(9):3649–56.

[23] Magaldi S, Mata-Essayag S, Hartung de Capriles C, Perez C, Colella MT, Olaizola C, et al. Well diffusion for antifungal susceptibility testing. Int J Infect Dis. 2004 Jan;8(1):39–45. PMID: 14690779. doi: 10.1016/j.ijid.2003.03.002.

[24] Tang XJ, Huang KM, Gui H, Wang JJ, Lu JT, Dai LJ, et al. Pluronic-based micelle encapsulation potentiates myricetin-induced cytotoxicity in human glioblastoma cells. Int J Nanomed. 2016 Oct 3;11:4991–5002. PMID: 27757032; PMCID: PMC5055108. doi: 10.2147/IJN.S114302.

[25] Lee S, Suh YJ, Lee Y, Yang S, Hong DG, Thirumalai D, et al. Anti-inflammatory effects of the novel barbiturate derivative MHY2699 in an MPTP-induced mouse model of Parkinson's disease. Antioxidants. 2021;10:1855. doi: 10.3390/antiox10111855.

[26] Karthikeyan C, Varaprasad K, Akbari-Fakhrabadi A, Hameed ASH, Sadiku R. Biomolecule chitosan, curcumin and ZnO-based antibacterial nanomaterial, via a one-pot process. Carbohydr Polym. 2020;249:116825.

[27] Elderdery AY, Alzahrani B, Alanazi F, Hamza SM, Elkhalifa AM, Alhamidi AH, et al. Amelioration of human acute lymphoblastic leukemia (ALL) cells by ZnO-TiO_2-Chitosan-Amygdalin nanocomposites. Arab J Chem. 2022;15(8):103999.

[28] Xie L, Li A, Zhou S, Zhang M, Ding Y, Wang P. Photocatalytic performance of nano-$ZnTiO_3$ decorated with Ag/AgCl nanoparticles for degradation of the organic dyes. Res Chem Intermed. 2021;47(6):2373–91.

[29] Al-BiRuNi JIPF. Structure, morphology, and optical properties of ZnO: Mg thin film prepared by sol-gel spin coating method. J Ilm Pendidik fisika Al-Biruni. 2021;10(2):241–50.

[30] Srikant V, Clarke DR. On the optical band gap of zinc oxide. J Appl Phys. 1998;83(10):5447–51.

[31] Yao B, Shi H, Bi H, Zhang L. Optical properties of ZnO loaded in mesoporous silica. J Physics: Condens Matter. 2000;12(28):6265.

[32] Ocakoglu K, Mansour SA, Yildirimcan S, Al-Ghamdi AA, El-Tantawy F, Yakuphanoglu F. Microwave-assisted hydrothermal synthesis and characterization of ZnO nanorods. Spectrochim Acta Part A: Mol Biomol Spectrosc. 2015;148:362–8.

[33] Pucci C, Martinelli C, Ciofani G. Innovative approaches for cancer treatment: current perspectives and new challenges. Ecancermedicalscience. 2019;13:961. doi: 10.3332/ecancer.2019.961.

[34] Ventola CL. The antibiotic resistance crisis: part 1: causes and threats. Pharm Therapeutics. 2015;40(4):277–83.

[35] Nanayakkara AK, Boucher HW, Fowler VG Jr, Jezek A, Outterson K, Greenberg DE. Antibiotic resistance in the patient with cancer: Escalating challenges and paths forward. CA

Cancer J Clin. 2021 Nov;71(6):488–504. doi: 10.3322/caac.21697.

[36] Mohamad Sukri SNA, Shameli K, Mohamed Isa ED, Ismail NA. Green synthesis of zinc oxide-based nanomaterials for photocatalytic studies: A mini-review. IOP Conf Ser Mater Sci Eng. 2021;1051:012083.

[37] Youssef AM, El-Sayed SM, El-Sayed HS, Salama HH, Assem FM, Abd El-Salam MH. Novel bionanocomposite materials used for packaging skimmed milk acid coagulated cheese (Karish). Int J Biol Macromol. 2018;115:1002–11.

[38] Barreto PL, Pires AT, Soldi V. Thermal degradation of edible films based on milk proteins and gelatin in inert atmosphere. Polym Degrad Stab. 2003;79(1):147–52.

[39] Youssef AM, El-Sayed HS, Islam EN, El-Sayed SM. Preparation and characterization of novel bionanocomposites based on garlic extract for preserving fresh Nile tilapia fish fillets. RSC Adv. 2021;11:22571.

[40] Bhatia R. Targeting leukemia stem cell resistance in chronic myelogenous leukemia. Trans Am Clin Climatol Assoc. 2019;130:246–54.

[41] Vamanu CI, Cimpan MR, Høl PJ, Sørnes S, Lie SA, Gjerdet NR. Induction of cell death by TiO_2 nanoparticles: studies on a human monoblastoid cell line. Toxicol Vitro. 2008;22(7):1689–96.

[42] Bentires-Alj M, Barbu V, Fillet M, Chariot A, Relic B, Jacobs N, et al. NF-kappaB transcription factor induces drug resistance through MDR1 expression in cancer cells. Oncogene. 2003 Jan 9;22(1):90–7. PMID: 12527911. doi: 10.1038/sj.onc.1206056.

[43] Ferro C, Florindo HF, Santos HA. Selenium nanoparticles for biomedical applications: From development and characterization to therapeutics. Adv Healthc Mater. 2021 Aug;10(16):e2100598. Epub 2021 Jun 13 PMID: 34121366. doi: 10.1002/adhm.202100598.